Light Harvesting Complex II B850 Excitation Dynamics

Johan Strümpfer and Klaus Schulten

Center for Biophysics and Computational Biology and
Beckman Institute, University of Illinois at Urbana-Champaign

Abstract

The dynamics of excitation energy transfer within the B850 ring of light harvesting complex 2 from *Rhodobacter sphaeroides* and between neighboring B850 rings is investigated by means of dissipative quantum mechanics. The assumption of Boltzmann populated donor states for the calculation of inter-complex excitation transfer rates by generalized Förster theory is shown to give accurate results since intra-complex exciton relaxation to near-Boltzmann population exciton states occurs within a few ps. The primary channels of exciton transfer between B850 rings are found to be the five lowest-lying exciton states, with non-850 nm exciton states making significant contributions to the total transfer rate.

The article appeared in **J. Chem. Phys., 131, 255101 (2009)** and may be downloaded from http://link.aip.org/?jpc/131/255101

1 Introduction

Light harvesting in plants and bacteria is achieved through the absorption of light by antenna pigment-protein complexes and subsequent energy transfer events, yielding increasingly more stable forms of energy.[1,2] In the case of purple bacteria, one of the simplest photosynthetic lifeforms, photons are absorbed by light harvesting complexes to arrive in the form of so-called excitons at a photosynthetic reaction center (RC), where the light energy is used for charge separation that causes an electron gradient across the bacterial cell membrane.[3,4]

The light harvesting proteins of the purple bacteria chromatophore include light harvesting complex 1 (LH1), light harvesting complex 2 (LH2) and RC complexes (shown in Figure 1). The chromatophore of *Rhodobacter sphaeroides* consists of pools of LH2 complexes that surround dimeric LH1-RC core complexes.[5] LH2 is the primary antenna complex of the chromatophore, not only due to its relative abundance, but also because of its large absorption cross-section.[6] The carotenoid (Car) and bacteriochlorophyll (BChl) molecules in the antenna complexes are the pigments

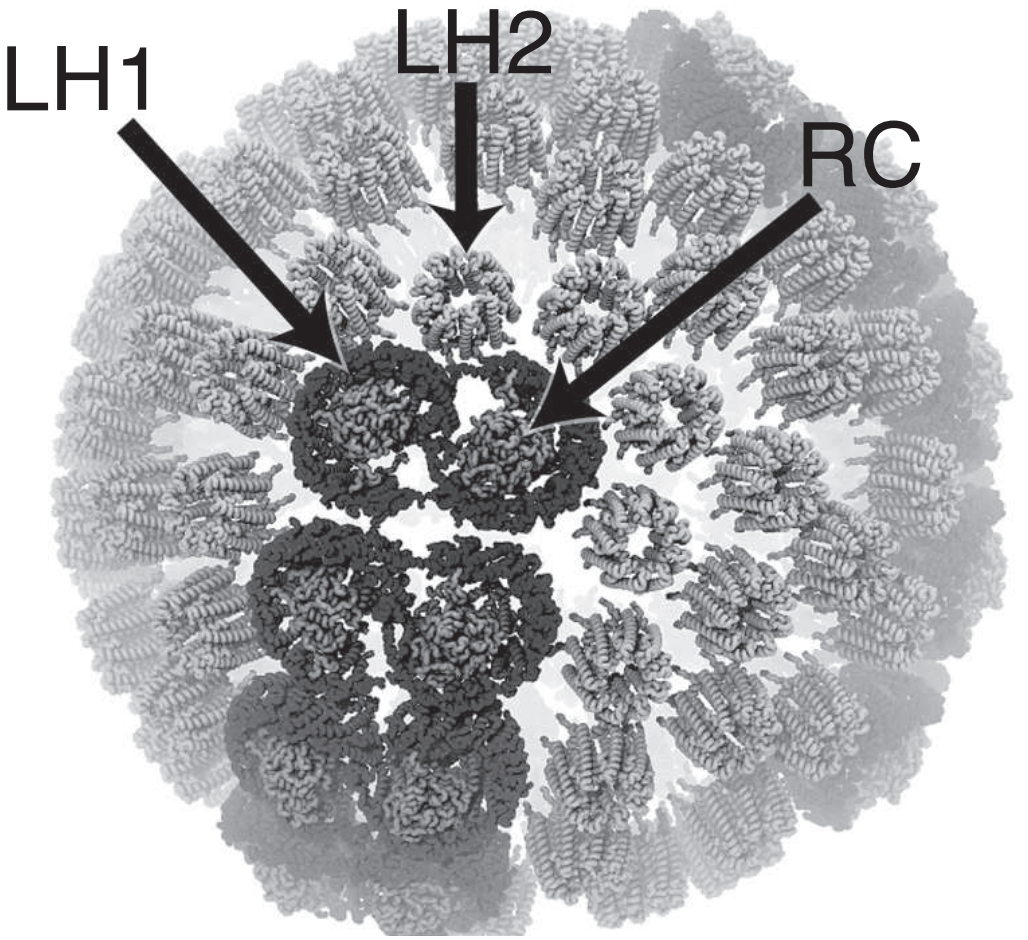

Figure 1: Patch of the chromatophore from purple photosynthetic bacteria *Rhodobacter sphaeroides* showing the placement of LH2 and LH1-RC complexes as determined from atomic force microscopy and computational modelling.[5] Pools of LH2 antenna complexes are seen to surround the LH1-RC core complexes; lipids are not shown. As the primary antennae of the chromatophore most of the inter-complex excitation transfer occurs between LH2s.

responsible for the absorbption of light and subsequent excitation transfer events.[7–9] On initial absorption of

light by the pigments of an LH2, the excitation energy is passed between LH2, LH1 and RC complexes. At the RC, the energy is used for charge separation, thus forming an electrical gradient across the membrane and initiating the next, more stable, phase in photosynthetic energy trapping.[10]

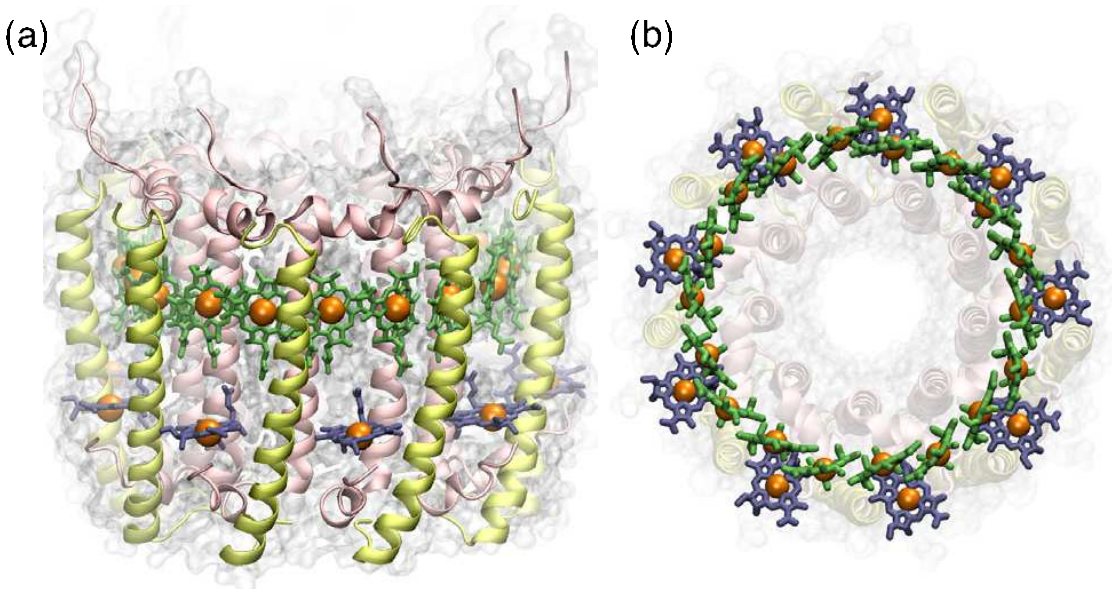

Figure 2: (a) The structure of LH2 showing the α- and β-subunits of each $\alpha\beta-$dimer in yellow and pink, respectively, the B850 Bchls in green and the B800 Bchls in blue. The cytoplasmic side is on the bottom. (b) Eighteen Bchls (green) form the so-called B850 ring and 9 Bchls (blue) form the so-called B800 ring. Nine carotenoid molecules also present are not shown.

LH2 (shown in Figure 2a) is formed by a ring of nine copies of a heterodimer of membrane span-

ning helices named α and β.[11] Bound to each $\alpha\beta$-heterodimer are 3 Bchls and 1 Car for a total of 36 pigments in LH2.[12] The near-IR absorption spectrum of LH2 shows two distinct peaks, due to the BChls in the complex, at 800 nm and 850 nm.[13] The 800 nm and 850 nm peaks are due to the Q_Y excited states of Bchls located in the B800 and B850 rings of LH2, shown in Figure 2b. The BChls in the B800 band are sufficiently far apart so that they interact only weakly with each other, thus each absorbs individually.[11] The BChls of the B850 ring are tightly packed, with center-to-center distances of less than 1 nm, and thus interact strongly with each other to form delocalized exciton states, shifting the absorption peak of the ring to 850 nm.[13] Energy that is absorbed by the B800 Bchls or Cars is quickly transferred to the B850 exciton states which then transfer to exciton states of nearby LH2 and LH1 complexes.[14] With an accurate description of the excitation dynamics within the B850 ring and of the excitation transfer between B850 rings, insight into the function of an improtant component of the purple bacteria light harvesting system is gained.

Prior theoretical investigations of the excitation

dynamics of LH2 used Redfield and Förster theories[15–19] and compared results with spectroscopic measurements. Redfield theory describes the excitation dynamics of a system where the environment coupling is significantly weaker than the coupling between pigments. Förster theory is used to calculate the transfer rate between pigments that are strongly coupled to the environment, but are weakly coupled to each other.[20,21] The conclusion has been drawn that due to the coherence between nearby Bchls, Förster theory cannot account for the excitation dynamics within a B850 ring.[20,22–24] It has been suggested also recently that Redfield theory cannot adequately describe the coherence dynamics in quantum systems[25] thus neither description may be sufficient to describe the excitation dynamics of LH2.

The coupling between BChls of different light harvesting complexes is much weaker than the coupling to the environment. Förster theory thus provides am accurate description for the inter-complex transfer rates and overall quantum efficiencies of chromatophores.[5,11] An important assumption is that the timescale of the intra-ring thermal relaxation is suffi-

ciently short to assume it to be instantaneous in comparison with inter-ring excitation transfer. This implies that excitation transfer between LH2 rings arises from Boltzmann-weighted intra-ring exciton states, an assumption which underlies the generalized Förster transfer theory.[26]

An accurate description of the overall excitation dynamics in LH2 requires that the environment and both the intra-ring and inter-ring couplings be treated nonperturbatively. In recent years a description of quantum dynamics in a noisy environment has been derived to arbitrary order in system-environment coupling by utilizing a hierarchy of auxiliary density matrices.[27,28] This method has been used to study the coherence dynamics in the Fenna-Matthews-Olsen pigment-protein complex of green sulphur bacteria.[29] The present study is, to the best of the authors' knowledge, the first application of the hierarchical equations of motion to a system as large as two B850 rings. It is the aim of the present study to explore the intra- and inter-ring excitation dynamics of the B850 ring and to investigate the assumptions underlying generalized Förster theory.

In Section II the theoretical description of the system as well as that of generalized Förster theory and

the hierarchy of equations of motion describing the quantum dynamics is given. Section III presents the excitation dynamics of a single B850 ring with initial states corresponding to a singly excited BChl and to an 850 nm delocalized state. In Section IV the excitation transfer between two B850 rings is investigated and the contributions of various excited states of the B850 ring to the inter-complex transfer rate is presented.

2 Method

The B850 ring is the system of interest and is described by the Hamiltonian

$$H_S = \sum_{i=1}^{N} E_i \left|i\right\rangle \left\langle i\right| + \sum_{i=1}^{N}\sum_{j=1}^{N} V_{ij} \left|i\right\rangle \left\langle j\right|, \qquad (1)$$

where $\left|i\right\rangle$ represents a localized excitation on BChl i, E_i is the Q_Y excitation energy, and the electronic coupling between excited states is given by V_{ij}. The system Hamiltonian H_S can be diagonalized to give the exciton spectrum ϵ_ν and associated exciton states $\left|\widetilde{\epsilon_\nu}\right\rangle = \sum_i C_\nu^i \left|i\right\rangle$.

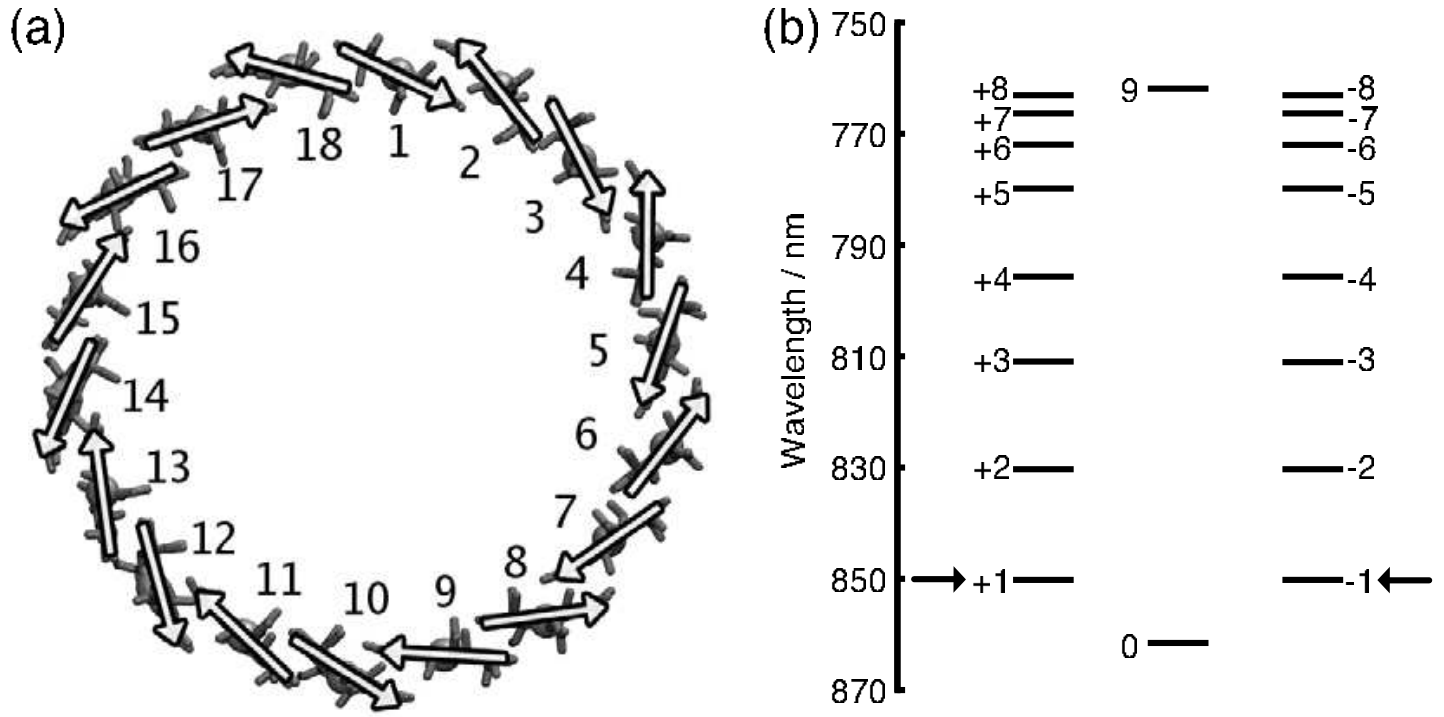

Figure 3: (a) B850 ring showing the alternating transision dipole moment orientations giving rise to the 9-fold symmetry. The arrows placed over the Mg atoms show the transition dipole moments from the N_B atom to the N_D atom of each Bchl.[11] (b) Exciton spectrum of B850 shown with the familiar k-labels.[30] The arrows indicate the two states with the highest oscillator strength, the so-called 850 nm states.

The B850 ring contains Bchls ($N = 18$) that are dimerized to give it a nine-fold symmetry as shown in Figure 3a. The interactions within a dimer and between two dimers thus specify all the nearest neighbour entries in H_S. Due to their close proximity, electrostatic

interaction alone cannot account for the nearest neighbour Bchl couplings.

Quantum chemistry calculations suggest the coupling V_{ij} between neighbouring Bchls in a dimer, e.g. V_{12}, as 363 cm^{-1} and between dimers, e.g. V_{23}, as 320 cm^{-1}.[5,31] The electrostatic environment in the dimer causes the Q_Y excited states of each Bchl to be shifted; alternating site energies E_j of 12457.66 cm^{-1} and 12653.66 cm^{-1} reproduce the 850 nm absorption peak in the exciton spectrum.[10] The non-nearest neighbour couplings V_{jk} are calculated using the induced dipole-induced dipole interaction

$$V_{ij} = C\frac{\mathbf{d}_i \cdot \mathbf{d}_j - 3\left(\mathbf{d}_i \cdot \hat{\mathbf{r}}_{ij}\right)\left(\mathbf{d}_j \cdot \hat{\mathbf{r}}_{ij}\right)}{\left|\mathbf{r}_{ij}\right|^3}. \qquad (2)$$

The coupling constant $C = 348000$ Å^{3}cm^{-1} is chosen to reproduce the LH2 exciton spectrum shown in Figure 3b.[5] The exciton spectrum consists of 8 degenerate states labelled with quantum numbers $k = \pm 1, \pm 2, \cdots, \pm 8$, and two non-degenerate states $k = 0$ and $k = 9$, the lowest and highest energy states respectively. States $k = \pm 1$, the so-called 850 nm states, contain 89% of the total oscillator strength and produce the 850 nm peak in the absorption spectrum.

Generalized Förster theory calculates the transfer rate between state ν of donor ring D to state μ of acceptor ring A as $(\beta = 1/k_B T)$

$$K_{\nu\mu} = \frac{2\pi}{\hbar} \frac{\exp\left(-\beta\epsilon_\nu\right)}{\sum_\alpha \exp\left(-\beta\epsilon_\alpha\right)} \times \sum_{i=1}^{N_D} \sum_{j=1}^{N_A} V_{ij}^2 \left|C_\nu^i\right|^2 \left|C_\mu^j\right|^2 J_{DA}^{\nu\mu}. \quad (3)$$

The spectral overlap $J_{DA}^{\nu\mu}$ between donor state ν and acceptor state μ is

$$J_{DA}^{\nu\mu} = \int dE S_D^\nu(E) S_A^\nu(E), \quad (4)$$

for the normalized donor and acceptor spectral lineshapes $S_D^\nu(E)$ and $S_A^\nu(E)$. The total transfer rate between the donor and acceptor is calculated as the sum over all states, $K = \sum_\nu \sum_\mu K_{\mu\nu}$.

The total Hamiltonian of system and bath is given by

$$H = H_S + H_B + H_{SB}, \quad (5)$$

with the three terms describing the system, bath and system-bath interaction, respectively. The bath is mod-

eled as a collection of harmonic oscillators,

$$H_B = \sum_{\xi} \left(\frac{p_\xi^2}{2m_\xi} + \frac{m_\xi \omega_\xi^2 x_\xi^2}{2} \right), \tag{6}$$

which are independently coupled to the Q_Y excited state of each BChl. The interaction between system and bath is assumed to be linear, namely

$$H_{SB} = \sum_{j=1}^{N} |j\rangle \langle j| \sum_{\xi} c_{j\xi} x_\xi. \tag{7}$$

The evolution of the total system from an arbitrary state can be accounted for by the total statistical operator

$$W = \rho \otimes R, \tag{8}$$

where ρ is the density operator of the system degrees of freedom and R is the density operator of the bath degrees of freedom.[32] The initial state of the system is given by

$$W(0) = \rho(0) \otimes \exp(-\beta H_B)/\mathrm{tr}_B \exp(-\beta H_B). \tag{9}$$

This corresponds to a factorized initial state which has been shown to lead to unphysical results in some

cases[33,34]. In the case of excitation dynamics, however, the factorized initial condition is valid since it arises from photon induced ground state to excited state transition in accordance with the Franck-Condon principle.[28]

The bath averaged operator $\langle O \rangle_B$ can be calculated by taking the trace of O over the bath degrees of freedom

$$\langle O \rangle_B = \mathrm{tr}_B(O e^{-\beta H_B})/\mathrm{tr}_B(e^{-\beta H_B}). \qquad (10)$$

The time evolution of the system density matrix $\rho(t)$ can be calculated by taking the bath average of the total statistical operator $W(t)$. This is evaluated as[35]

$$\begin{aligned} \rho(t) &= \langle W(t) \rangle_B \\ &= \left\langle \exp\left(-\frac{i}{\hbar} \int_0^t ds \mathcal{L}(s) \right) \right\rangle_B \rho(0). \end{aligned} \qquad (11)$$

A hierarchy of equations of motion arise by performing the bath average, exploiting the Gaussian nature of the harmonic bath and taking the derivative of the time evolution operator.[27,36,37]

Once the bath average is taken, its effect only enters through the correlation functions $C_j(t)$ of the bath

coupling operators $u_j = -\sum_\xi c_{j\xi} x_\xi$,

$$\begin{aligned} C_j(t) &= \langle u_j(t) u_j(0) \rangle_B \\ &= \frac{1}{\pi} \int_0^\infty d\omega J_j(\omega) \frac{\exp(-i\omega t)}{1 - \exp(-\beta\hbar\omega)}. \end{aligned} \quad (12)$$

It is important to note here that we assume each Bchl has an independent bath. The correlation function is calculated from the bath spectral density

$$J_j(\omega) = \frac{1}{\hbar} \sum_\xi \frac{c_{j\xi}^2}{2 m_\xi \omega_\xi} \delta(\omega - \omega_\xi). \quad (13)$$

In this work we employ a Drude spectral density given by

$$J_j(\omega) = 2 \frac{\lambda_j \gamma_j}{\hbar} \frac{\omega}{\omega^2 + \gamma_j^2}; \quad (14)$$

the corresponding correlation function is[38]

$$C_j(t) = \sum_{m=0}^{\infty} c_{j,m} \exp(-\nu_{j,m} t). \quad (15)$$

Here $\nu_{j,0} = \gamma_j$ is the Drude decay constant and $\nu_{j,m\geq 1} = 2\pi m / \beta\hbar$ are the Matsuraba frequencies[38]. The sum to infinity in (15) cannot be treated exactly

and is thus truncated at $m = M$. The coefficients in the correlation function are

$$c_{j,0} = \frac{\gamma_j \lambda_j}{\hbar} \left(\cot(\beta \hbar \gamma_j / 2) - i \right) \tag{16}$$

$$c_{j,m \geq 1} = \frac{4 \lambda_j \gamma_j}{\beta \hbar^2} \frac{\nu_{j,m}}{\nu_{j,m}^2 - \gamma_j^2} \tag{17}$$

The derivation of the hierarchy of equations of motion for this form of spectral density has been presented in previous publications[36,39–41] and for completeness is presented in Appendix A. From the time derivative of (11) using the Drude spectral density arises a hierarchy of auxiliary system density matrices indexed by $\mathbf{n} = (n_{1,0}, \cdots, n_{1,M}, \cdots, n_{N,0}, \cdots, n_{N,M})$ that are governed by the following equations of motion:

$$\begin{aligned} \partial_t \rho_{\mathbf{n}} = & -\frac{i}{\hbar} \left[H_s, \rho_{\mathbf{n}} \right] - \sum_{j=1}^{N} \sum_{m=0}^{M} n_j \nu_{j,m} \rho_{\mathbf{n}} \\ & - \sum_{j=1}^{N} \sum_{m=M+1}^{\infty} \frac{c_{j,m}}{\nu_{j,m}} \left[|j\rangle \langle j| , \left[|j\rangle \langle j| , \rho_{\mathbf{n}} \right] \right] \\ & - i \sum_{j=1}^{N} \sum_{m=0}^{M} \left[|j\rangle \langle j| , \rho_{\mathbf{n}_{j,m}^{+}} \right] \end{aligned}$$

$$-i\sum_{j=1}^{N}\sum_{m=0}^{M} n_{j,m}\left(c_{j,k}\left|j\right\rangle\left\langle j\right|\rho_{\mathbf{n}_{j,m}^{-}} -\rho_{\mathbf{n}_{j,m}^{-}}\left|j\right\rangle\left\langle j\right|c_{j,m}^{*}\right), \tag{18}$$

where the temperature correction term proposed by Ishizaki and Tanimura[36] to account for the truncation of the sum in (15) has been included. The correction term has been shown to significantly reduce the number of Matsuraba terms required for convergence[36,42].

The matrices are linked via $\mathbf{n}_{j,m}^{\pm} = (n_{1,0},\cdots,n_{j,m}\pm 1,\cdots,n_{N,M})$. Any matrix with a negative entry in the index vector $\mathbf{n}$ is set to zero. Each tier L of the hierarchy is defined through the sum over the indices in $\mathbf{n}$,

$$L=\sum_{j=1}^{N}\sum_{m=0}^{M} n_{j,m} \tag{19}$$

The matrix with index vector $\mathbf{n}=(0,\cdots,0)$, the only matrix in tier $L=0$, is the system density matrix that is of primary interest, while the higher tier matrices are auxiliary matrices that take into account the bath effects on the system.

The hierarchy of matrices can be visualised as the vertices in a Pascal simplex of dimensionality equal to the number of elements in $\mathbf{n}$. The total number of vertices in a simplex with dimensionality d up to and including those in tier L can be calculated iteratively using $n_{\mathrm{vert}}(d, L) = \sum_{k_d=1}^{L} n_{\mathrm{vert}}(d-1, k_d - 1)$.

The number of matrices in the hierarchy are infinite, thus a truncation scheme must be chosen. It has been shown that the hierarchy can be truncated at a tier L_{trunc} by setting all higher tier density matrices to zero, with the relevant dynamics of the sytem being unaffected.[28,36] L_{trunc} is typically too large for present computational resources and a lower tier truncation is often chosen.[28,43]

Accurate spectral densities have been determined for this system[44–46] and give rise to multiple exponential terms for the bath correlation function (indeed, each Lorentzian peak gives rise to two exponential terms). Each exponential term in the correlation function, however, increases the number of indices by a factor N. For systems as large as the B850 ring in LH2, such spectral densities translate into intractably large computation sizes for truncations greater than $L_{\mathrm{trunc}} = 1$, which corresponds to the time-nonlocal formalism of

dissipative quantum dynamics and is only second order in system-bath coupling.[43,47] The Drude spectral density, however, only gives rise to a single exponential term in the correlation function and hence larger values of L_{trunc} become computationally tractable.

The dynamics computed using the hierarchical equations of motion (18) is bath averaged. As mentioned previously, the bath only enters into the formulation via the spectral density, thus the choice of parameters is an important one to consider. The bath parameters that are input to the method are the bath response time $1/\gamma_j$ and the reorganisation energy λ_j. In general, these are site dependent but due to the symmetry and relative homogeneity within the ring we set $1/\gamma_j = 1/\gamma = 100$ fs and $\lambda_j = \lambda = 200$ cm^{-1} to match parameters determined from fits to spectroscopic data.[48,49]

Fourth order Runga-Kutta numerical integration with a 1 fs time-step was used to integrate the hierarchical equations of motion. For one B850 ring (18 BChls) using an eighth order system bath coupling ($L_{\mathrm{trunc}} = 4$) and two temperature correction terms, 424 270 matrices are required. Using double preci-

sion, this requires 12.3 Gb of memory. Two B850 rings with the same number of temperature correction terms and system-bath coupling uses 6 210 820 matrices (720 Gb memory). With a sixth order system-bath coupling ($L_{\mathrm{trunc}} = 3$) the number of matrices is reduced to 221 815 (26 Gb memory).

The integration code needed to be parallelized for long simulation times due to the large number of coupled matrix differential equations. Parallelization over multiple networked computers is inefficient due to the large memory requirement and the coupled structure of the hierarchy. Using multiple integration threads, each concerned with an equal number of matrices, on a multi-core shared memory computer the communication bottleneck was overcome. On a 16 cpu core shared memory computer with a cpu core speed of 2.7 Ghz, an integration time-step takes 23 seconds for a single B850 ring and 67 seconds for two B850 rings.

3 Results

3.1 Dynamics of a single B850 ring

Two simulations of the density matrix were perfomed for a single B850 ring at a temperature of 300K. The first was done with the initial state consisting of only a single excited BChl ($\rho_0 = |1\rangle\langle 1|$) and the second with the initial state given by the 850 nm ($k = +1$) state ($\rho_0 = |\widetilde{\epsilon_2}\rangle\langle\widetilde{\epsilon_2}|$). The coherence length of the system was computed at each time step as the inverse participation ratio, defined by[45]

$$L_\rho = \frac{1}{N}\frac{\left(\sum_{i,j}|\rho_{ij}|\right)^2}{\sum_{i,j}|\rho_{ij}|^2}. \tag{20}$$

The site dynamics, depicted in Figure 4a, shows the dissipation of the excitation across all sites from a single initially populated site. The strong coupling between neighbouring sites is reflected in the very fast population transfer between neighbouring sites. This is indicated by the rapid increase of BChl 2 population in Figure 4a. Excitation extends rapidly to neighboring sites. The transfer to neighbouring sites occurs in less

than 15 fs and transfer across half the ring occurs in about 65 fs.

The dissipation of the initial state, such that the site populations converge to their steady-state values, happens in about 0.4 ps. At the steady state the excitation is completely delocalized around the ring. The alternate Q_Y energies within the dimer cause alternating steady state populations of 0.067 and 0.044 such that the total steady-state population of each dimer is $1/9$.

The time evolution of the coherence length, shown in Figure 4b, presents in terms of a single quantity the evolution of the coherence terms in the density matrix. The initial coherence length is 1 since initially only a single BChl is occupied. The fast inter-site excitation dynamics is reflected in the rapid fluctuation of the coherence length up to ~ 0.2 ps. After 0.4 ps, once the site populations have reached their steady state values, the coherence terms are still building up to converge to their steady state values in about 1 ps. The final coherence length $L_\rho = 11.2$ is very close to the coherence length calculated for Boltzmann populated exciton states, namely $L_\rho = 11.4$.

The population of exciton state $|\widetilde{\epsilon_\nu}\rangle$ is calculated using $P_\nu(t) = \langle\widetilde{\epsilon_\nu}|\,\rho(t)\,|\widetilde{\epsilon_\nu}\rangle$. Figures 4c and 4d show

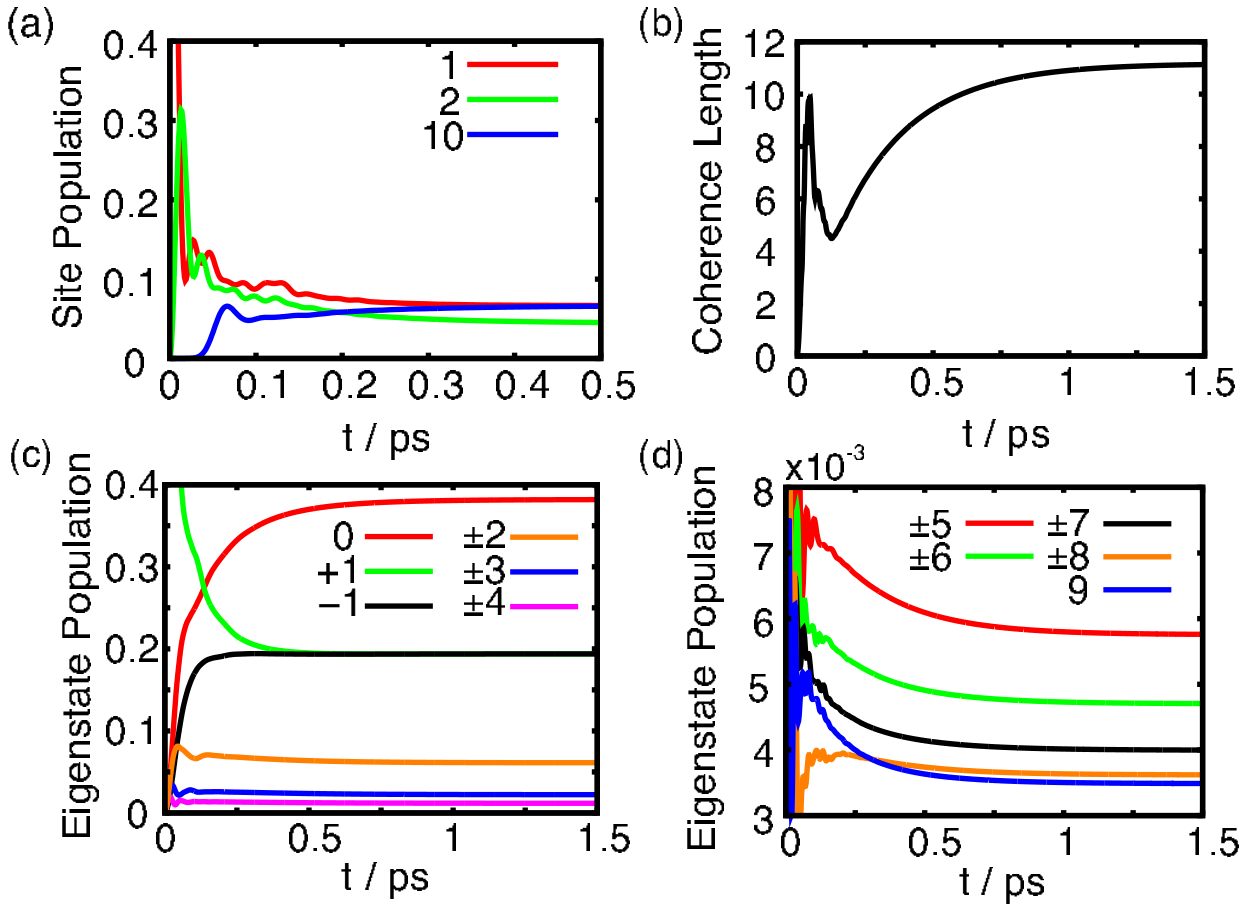

Figure 4: (a) Population dynamics of Bchls 1, 2 and 10 starting from $\rho_0 = |1\rangle\langle 1|$. The transfer of excitation across half the ring takes about 65 fs. The difference between neighbouring Bchl populations is seen by the steady state difference of BChls 1 and 2 and is due to the alternating site energies in the Hamiltonian. (b) Time evolution of the coherence length in the B850 ring as measured by the inverse participation ratio starting from $\rho_0 = |1\rangle\langle 1|$. The coherence length converges to $L_\rho = 11.2$. (c) Time evolution of the 9 lowest energy exciton states with $\rho(0) = |\widetilde{\epsilon_2}\rangle\langle\widetilde{\epsilon_2}|$. (d) Time evolution of the 9 highest energy exciton states starting from $\rho(0) = |\widetilde{\epsilon_2}\rangle\langle\widetilde{\epsilon_2}|$.

the evolution of the exciton states from the initial state $\rho(0) = |\widetilde{\epsilon_2}\rangle \langle \widetilde{\epsilon_2}|$. All states, but the initally excited state and the ground state, converge to their steady state values in 0.2 ps. The ground state and initially excited state converge to their steady state populations on a longer timescale of about 0.8 ps. These timescales match the times seen in Figures 4a and 4b for the fast population transfer and the longer build-up of the coherence. Similar bi-exponential timescales are noted in spectroscopic experiments for LH2[15,18,50,51] as well as LH1[52,53].

The steady-state populations at $t = 5$ ps are shown in Figure 5 along with the populations expected from Boltzmann distributed exciton states. The lowest-lying exciton states, particularly states $k = \pm 1, \pm 2$, assume populations that are close to Boltzmann weights and the overall distribution resembles a Boltzmann distribution. The same steady state is reached independently of the chosen initial state.

To test for convergence, the excitation dynamics of the B850 ring was also calculated using lower N_{trunc} values and fewer Matsuraba terms. Using a value of $N_{\mathrm{trunc}} = 1$ (time-nonlocal formalism) we found that the inter-site transfer times were identical, however the ex-

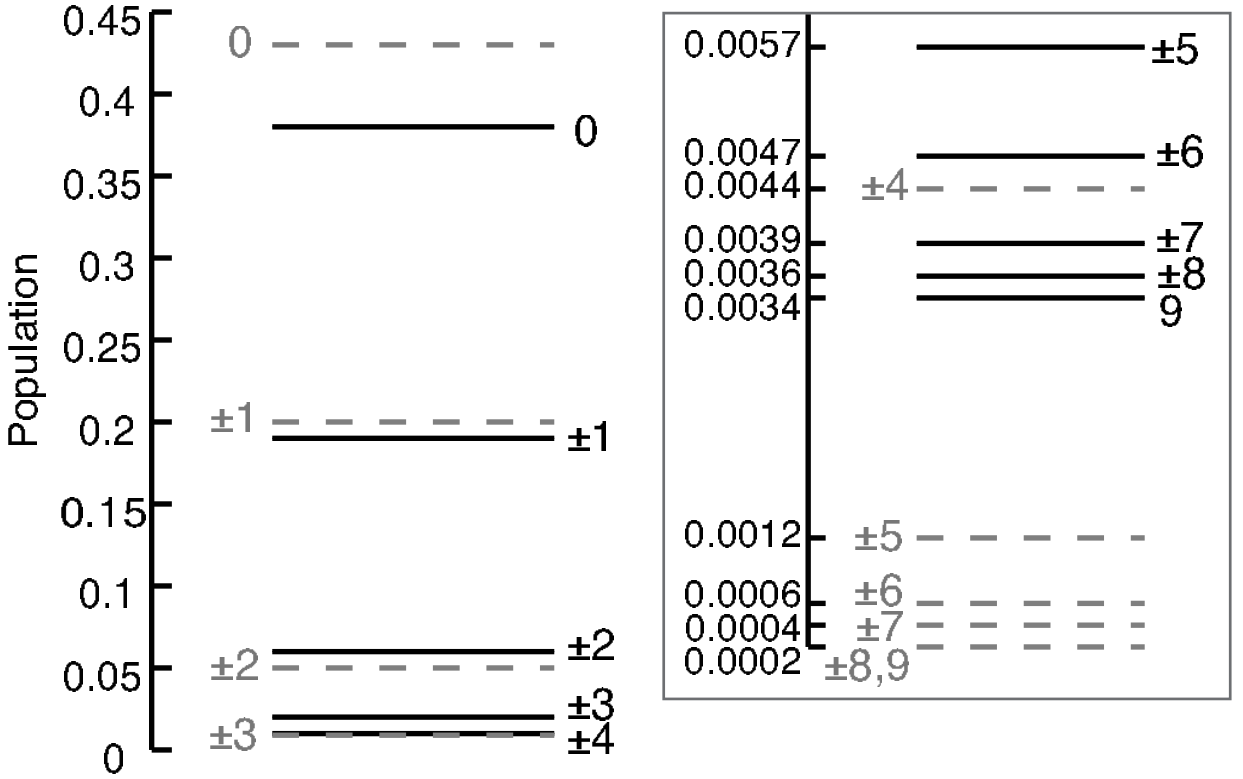

Figure 5: Steady state populations (solid lines) and Boltzmann populations (dashed lines) of the exciton states of LH2 B850. The inset shows the exciton populations of the highest energy states. The state labels on the left of the lines denote the Boltzmann populated states and the labels on the right denote the steady state populations.

citon populations' relaxation times were longer and the density matrix did not remain positive definite. With a cut-off of $N_{\mathrm{trunc}} = 3$ the times for inter-site transfer and exciton relaxation were very close to those seen with $N_{\mathrm{trunc}} = 4$. The relative difference between the

exciton steady state populations with $N_{\mathrm{trunc}} = 3$ compared to $N_{\mathrm{trunc}} = 4$ was 0.3% which indicates reasonable convergence with respect to the hierarchy truncation level. The inclusion of the temperature correction terms to the formalism greatly enhances convergence with respect to the number of Matsuraba terms required. The maximum relative difference for the exciton populations between including only 1 Matsuraba term and 2 terms is 0.7%, indicating reasonable convergence with respect to the number of included Matsuraba terms.

3.2 Dynamics of two B850 rings

The calculation of the excitation dynamics was repeated for two B850 rings (36 sites in total) at 300K. The rings were placed 85 Å apart (center-to-center distance), which corresponds to steric contact of the two LH2 proteins holding the B850 rings. The initial state was set to the $k = +1$ state on the donor ring $\rho(0) = |\epsilon_2\rangle\langle\epsilon_2|$. The dynamics on the donor ring closely echoed what is seen in Figures 4c and 4d. In the time it takes to reach the steady-state for a single ring, 10% of the total population is transfered to

the acceptor ring. Shown in Figure 6 is the transfer of population from the donor to the acceptor ring. The population transfer from the donor follows a single exponential decay with a decay time of 9.1 ps towards equal donor and acceptor population. Figure 6 indi-

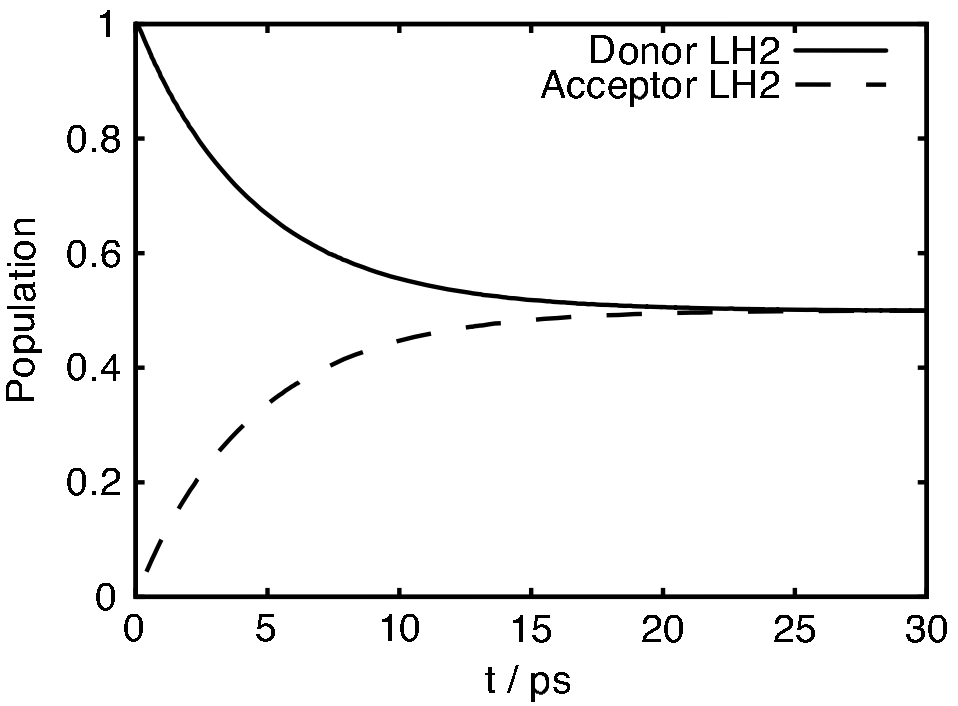

Figure 6: Transfer of excitation from donor to acceptor ring, showing single exponential decrease (increase) for the donor (acceptor). The tranfer time is 9.1 ps, the transfer time resulting from the generalized Förster calculation is 10.2 ps.

cates that the transfer between rings is incoherent and

can be described by the kinetic equation

$$\partial_t P = -kP + k\left(1 - P\right), \tag{21}$$

where P is the population of the donor ring. This implies that the inter-complex transfer rate can be accurately calculated using the generalized Förster formalism. Using generalized Förster theory the LH2 to LH2 transfer time is calculated to be 10.2 ps. If the near Boltzmann exciton populations shown in Figure 5 are used instead of Boltzmann populated exciton states, the transfer time is calculated to be 9.5 ps. The remaining difference between the transfer rates is less than the intra-ring relaxation time of ≈ 1 ps. Both results correspond well with the ps scale transfer time measured experimentally.[54]

In the calculations using the hierarchy method, not all sources of thermal noise have been taken into account. One such source arises in the protein environment from so-called static disorder[55,56] due to protein structural dynamics that occur on a timescale much longer than the excitation dynamics. The static disorder is responsibe for the inhomogeneous line-broadening in the fluorescence spectra[57], but is com-

putationally expensive to take into account in the hierarchy method. However, the effect of static disorder can easily be taken into account in the generalized Förster formalism; adding Gaussian diagonal disorder with $\sigma = 200$ cm^{-1} increases the transfer time by 2.2 ps (18%) from the non-disordered calculation, namely to 12.4 ps.

The superradiance effect of some of the exciton states ($k = 0, \pm 1$) has been shown to be enhanced by the spectral broadening from homogeneous and inhomogeneous disorder[49,56]. The exciton transfer between complexes is, however, not soleley dependent on the oscillator strengths of the exciton states (which characterize the superradiance effect), but also on the intercomplex couplings, the exciton state populations and the spectral overlap.

Since we have shown that the assumption of Boltzmann-distributed donor states is a reasonable approximation, we can proceed with a further investigation of the primary contributions to the intercomplex transfer rate whilst taking static disorder into account using generalized Förster theory.[58–61] When disorder is introduced it is not clear in genereal whether the character of individual exciton states of the averaged

complex is conserved. However, for the typical disorder seen in LH2 one can still identify the shifted exciton states throught their character seen without disorder. Indeed, Figure 7 demonstrates that the exciton states retain their labelling with the inclusion of disorder.[30,49]

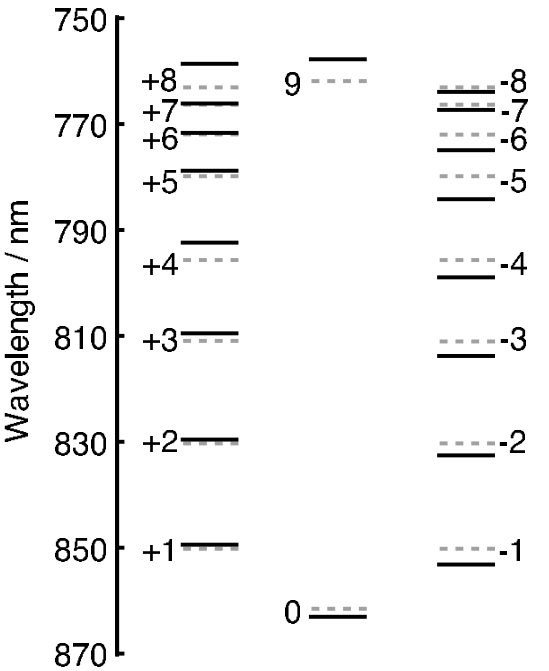

Figure 7: Distortion of B850 exciton states due to Gaussian diagonal disorder. The dashed lines correspond to the exciton spectrum of the averaged B850 ring showing the degeneracy for all the states with the exception of the $k = 0$ and $k = 9$ states. The solid lines show the exciton spectrum of a single realisation of Gaussian diagonal disorder with a width $\sigma = 200$ cm^{-1}. With the inclusion of disorder, the degeneracies are lifted, yet the exciton states of the disordered Hamiltonian can be linked to those of the ideal Hamiltonian (c.f. Fig. 3b).

Table 1 lists the individual transfer rates of the disordered systems. The five lowest energy exciton states contain 98% of the total transfer rate. The states with the highest oscillator strength, have 39% of the total exciton population and contribute 69% of the total transfer rate with the inclusion of disorder. The remaining three states, labelled by $k = 0, +2, -2$, each contribute 8%,12% and 8%, respectively. As would be expected, the degeneracy in the exciton states is lifted with the inclusion of disorder, which is clearly shown through the different Boltzmann populations of the $k = \pm 1$ and $k = \pm 2$ states.

4 Discussion

The excitation dynamics within one B850 ring of LH2 and between two B850 rings have been computed using the hierarchical equations of motion[36] for a quantum system in contact with a thermal bath. Within one B850 ring two timescales for the excitation dynamics were observed, 0.2 ps and 1 ps, corresponding to the relaxation of site populations and coherence terms, respectively. It was shown that the relaxation within a

Table 1: Boltzmann populations of the exciton states of a B850 ring along with the transfer rates from these states to another B850 ring, averaged over 10 000 realisations of diagonal disorder.

State	Boltzmann Population	Transfer Rate (ps^{-1})	% of Total Rate
0	0.47	1/161	8
+1	0.23	1/35	36
-1	0.16	1/38	33
+2	0.06	1/102	12
-2	0.04	1/145	9
+3	0.01	1/807	1
-3	0.01	1/1244	1
Total	1	1/12.4	100

single B850 ring happens on a much faster timescale (~ 1 ps) compared to the excitation transfer timescale (~ 10 ps) between two B850 rings. Excitation transfer between two rings exhibits single exponential kinetics, indicating incoherent transfer. This substantiates that generalized Förster theory provides an accurate de-

scription of exciton migration between complexes and can furnish quantitative predictions of excitation transfer rates between light harvesting complexes.

The effect of static disorder on the intra-ring excitation dynamics could not be characterized in the framework of the hierarchy calculations. Previous work accounted for intra-ring excitation dynamics including static disorder using Redfield theory. In this case transfer rate across half the ring for LH2 range between 100 and 350 fs for different realisations of disorder.[18,62] The comparison of these times with those determined here (c.f. Fig. 4a) provides a good indication of the effect of static disorder on the intra-ring excitation dynamics.

The inclusion of static disorder on tranfer between B850 rings was investigated employing generalized Förster theory. Diagonal static disorder increased the transfer time by only 2.2 ps, indicating an inherent accomodation of disorder that is to be expected in robust biological systems. It was found that the five lowest lying exciton states are responsible for 98% of the energy transfer between rings. The primary contributors are the $k = \pm 1$ states due to their high oscillator strength, however states $k = 0, \pm 2$ make non-negligble contributions to the total transfer rate. This

has been noted previously and is due to the exciton populations of the $k = 0, \pm 2$ and the mixing of these states with the $k = \pm 1$ states[63].

Freiberg et al. have shown that the thermal baths of BChls in the B850 ring may be correlated.[49] The effect of different bath parameters and of correlated bath modes between BChls are currently being investigated.

5 Acknowledgements

This work was supported by grants from the National Science Foundation (MCB-0744057) and National Institute of Health (P41-RR05969). The authors thank Melih Şener for helpful insights and discussions.

6 Appendix A

6.1 Derivation Of Hierarchy

The derivation of the hierarchy of equation of motion furnished here follows references[36] and[37] for a general

system-bath interaction Hamiltonian given by

$$H_{SB} = -\sum_j V_j u_j, \tag{22}$$

where V_j are the system operators and u_j are the bath operators. The hierarchy of equation of motion arises by taking the time derivative of the bath averaged Liouville space propogator. The time evolution of the density matrix is calculated from

$$\begin{aligned} \rho(t) &= \left\langle \exp\left(-\frac{i}{\hbar}\int_{t_i}^{t} ds \mathcal{L}(s)\right)\right\rangle_B \rho(t_i) && (23) \\ &= \langle \mathcal{U} \rangle_B \rho(t_i). && (24) \end{aligned}$$

The Liouville space propogator $\mathcal{U}$ can be expressed in path integral form, however a representation needs to be chosen. Choosing an arbitrary Liouville space representation $\mathbf{q} = (q, q')$, the path integral form of the propogator is (setting $\hbar = 1$)[64]

$$\begin{aligned} &\mathcal{U}\left[\mathbf{q}_f(t); \mathbf{q}_i(t_i)\right] = \\ &\int_{\mathbf{q}_i(t_i)}^{\mathbf{q}_f(t)} \mathcal{D}\mathbf{q}\, e^{i\mathcal{S}[q]}\, \mathcal{F}_{\mathrm{FV}}\left[\mathbf{q}(t)\right] e^{-i\mathcal{S}\left[q'\right]}, \end{aligned} \tag{25}$$

where $\mathcal{S}[q]$ is the classical action along path q of the system and $\mathcal{F}_{\mathrm{FV}}[\mathbf{q}(t)]$ is the Feynman-Vernon influence functional where the bath enters the formulation. Feynman showed that by employing stochastic bath variables that obey Gaussian statistics, the bath averaged influence functional can be written in terms of the bath correlation function $\langle u_j(t)u_j(\tau)\rangle = C_j(t-\tau)$ as [64]

$$\begin{aligned}\mathcal{F}_{\mathrm{FV}}[\mathbf{q}(t)] &= \exp\Bigg\{-\sum_j \int_{t_i}^{t} d\tau \,(V_j[q(\tau)] \\ &\qquad -V_j[q'(\tau)]) \\ &\qquad \times \left(\widetilde{V}_j[q(\tau)] - \widetilde{V}_j^*[q'(\tau)]\right)\Bigg\},\end{aligned} \tag{26}$$

where * represents the complex conjugate and the following notation has been introduced

$$\widetilde{V}_j[q(\tau)] = \int_{t_i}^{t} d\tau C_j(t-\tau)\, V_j[q(\tau)]\,. \tag{27}$$

To simplify notation, the Liouville space commutator is introduced for an arbitrary operator $\mathcal{O}$

$$\mathcal{O}^{\times}[\mathbf{q}] = \mathcal{O}[q] - \mathcal{O}^{\dagger}[q']\,, \tag{28}$$

where $\mathcal{O}^\dagger$ is the Hermitian conjugate of $\mathcal{O}$. The influence functional is thus written as:

$$\mathcal{F}_{\mathrm{FV}}\left[\mathbf{q}(t)\right] = \exp\left\{-\sum_j \int_{t_i}^{t} d\tau V_j^{\times}\left[\mathbf{q}(\tau)\right] \widetilde{V}_j^{\times}\left[\mathbf{q}(\tau)\right]\right\}, \quad (29)$$

To proceed, the time derivative of the influence functional is considered:

$$\partial_t \mathcal{F}_{\mathrm{FV}}\left[\mathbf{q}(t)\right] = -\sum_j V_j^{\times}\left[\mathbf{q}(t)\right] \widetilde{V}_j^{\times}\left[\mathbf{q}(t)\right] \mathcal{F}_{\mathrm{FV}}\left[\mathbf{q}(t)\right]. \quad (30)$$

By introducing *auxiliary* influence functionals

$$\mathcal{F}_{j_1}\left[\mathbf{q}(t)\right] = \left(-i\widetilde{V}_{j_1}^{\times}\left[\mathbf{q}(t)\right]\right) \mathcal{F}_{\mathrm{FV}}\left[\mathbf{q}(t)\right], \quad (31)$$

the time derivative can be re-written as

$$\partial_t \mathcal{F}_{\mathrm{FV}}\left[\mathbf{q}(t)\right] = -i\sum_{j_1} V_{j_1}^{\times}\left[\mathbf{q}(t)\right] \mathcal{F}_{j_1}\left[\mathbf{q}(t)\right]. \quad (32)$$

The subscript 1 in the summation index indicates that the auxiliary influence functional is of tier 1. Taking the time derivative of $\mathcal{F}_{j_1}\left[\mathbf{q}(t)\right]$ gives,

$$\partial_t \mathcal{F}_{j_1}\left[\mathbf{q}(t)\right] = -i\left(\partial_t \widetilde{V}_{j_1}^{\times}\left[\mathbf{q}(t)\right]\right) \mathcal{F}_{\mathrm{FV}}\left[\mathbf{q}(t)\right]$$

$$-i\sum_{j_2}\left\{V_{j_2}^{\times}\left[\mathbf{q}(t)\right]\left(-i\widetilde{V}_{j_1}^{\times}\left[\mathbf{q}(t)\right]\right)\right.$$
$$\left.\times\left(-i\widetilde{V}_{j_2}^{\times}\left[\mathbf{q}(t)\right]\right)\mathcal{F}_{\mathrm{FV}}\left[\mathbf{q}(t)\right]\right\}. \quad (33)$$

The second term arising from the derivative of $\mathcal{F}_{\mathrm{FV}}\left[q,q'\right]$ introduces a new set of auxiliary influence functionals

$$\mathcal{F}_{j_1 j_2}\left[\mathbf{q}(t)\right]=\left(-i\widetilde{V}_{j_1}^{\times}\left[\mathbf{q}(t)\right]\right)$$
$$\times\left(-i\widetilde{V}_{j_2}^{\times}\left[\mathbf{q}(t)\right]\right)\mathcal{F}_{\mathrm{FV}}\left[\mathbf{q}(t)\right]. \quad (34)$$

The time derivative of $\partial_t\widetilde{V}_{j_1}^{\times}\left[\mathbf{q}(t)\right]$ can be calculated

$$\partial_t\widetilde{V}_{j_1}^{\times}\left[\mathbf{q}(t)\right]=\left(C_{j_1}(0)V_{j_1}\left[\mathbf{q}(t)\right]\right)^{\times}$$
$$\times\int_{t_i}^{t}d\tau\left(\partial_t C_{j_1}(t-\tau)V_{j_1}\left[\mathbf{q}(\tau)\right]\right)^{\times}. \quad (35)$$

To proceed with calculating (33), a form of the correlation function is needed. Inserting equation (15) into (35) gives

$$\partial_t\widetilde{V}_{j_1}^{\times}\left[\mathbf{q}(t)\right] \quad = \quad \sum_m\left(c_{j_1,m}V_{j_1}\left[\mathbf{q}(t)\right]\right)^{\times}$$

$$+\sum_{m}\gamma_{j_1,m}\widetilde{V}_{j_1}^{\times}\left[\mathbf{q}(t)\right]. \quad (36)$$

The derivative of a tier 1 auxiliary influence functional is then expressed as

$$\begin{aligned}\partial_t\mathcal{F}_{j_1}\left[\mathbf{q}(t)\right] &= -i\sum_{m}\left(c_{j_1,m}V_{j_1}\left[\mathbf{q}(t)\right]\right)^{\times}\mathcal{F}_{\mathrm{FV}}\left[\mathbf{q}(t)\right]\\ &\quad -\sum_{m}\gamma_{j_1,m}\mathcal{F}_{j_1}\left[\mathbf{q}(t)\right]\\ &\quad -i\sum_{j_2}V_{j_2}^{\times}\left[\mathbf{q}(t)\right]\mathcal{F}_{j_1j_2}\left[\mathbf{q}(t)\right]. \quad (37)\end{aligned}$$

The time derivative of a tier 1 auxiliary functional is then determined by the tier 0 influence functional $\mathcal{F}_{\mathrm{FV}}\left[\mathbf{q}(t)\right]$, the same tier 1 auxiliary influence function $\mathcal{F}_{j_1}\left[\mathbf{q}(t)\right]$ and the tier 2 auxiliary influence functionals $\mathcal{F}_{j_1j_2}\left[\mathbf{q}(t)\right]$.

Equations (31) and (34) lead to a general definition for the auxiliary influence functionals, where for the index vector $\mathbf{n}$ defined in the text, the corresponding auxiliary influence functional can be defined as

$$\mathcal{F}_{\mathbf{n}}\left[\mathbf{q}(t)\right]=\prod_{j,m}\left(-i\widetilde{V}_{j}^{\times}\left[\mathbf{q}(t)\right]\right)^{n_{j,m}}\mathcal{F}_{\mathrm{FV}}\left[\mathbf{q}(t)\right]. \quad (38)$$

The time derivative of this is

$$\begin{aligned}\partial_t \mathcal{F}_{\mathbf{n}}\left[\mathbf{q}(t)\right] = & -\sum_{j,m} n_{j,m}\nu_{j,m}\mathcal{F}_{\mathbf{n}}\left[\mathbf{q}(t)\right] \\ & -i\sum_{j,m} V_j^{\times}\left[\mathbf{q}(t)\right]\mathcal{F}_{\mathbf{n}_{j,m}^{+}}\left[\mathbf{q}(t)\right] \\ & -i\sum_{j,m} n_{j,m}\left(c_{j,m}V_j\left[\mathbf{q}(t)\right]\right)^{\times}\mathcal{F}_{\mathbf{n}_{j,m}^{-}}\left[\mathbf{q}(t)\right].\end{aligned} \tag{39}$$

Defining further the auxiliary propogators

$$\mathcal{U}_{\mathbf{n}}\left[\mathbf{q_f}(t),\mathbf{q_i}(t_i)\right] = \int_{\mathbf{q}_i(t_i)}^{\mathbf{q}_f(t)} \mathcal{D}\mathbf{q} e^{i\mathcal{S}[q]}\mathcal{F}_{\mathbf{n}}\left[\mathbf{q}(t)\right]e^{-i\mathcal{S}\left[q'\right]}, \tag{40}$$

and auxiliary density matrices

$$\rho_{\mathbf{n}}(t) = \mathcal{U}_{\mathbf{n}}\left[\mathbf{q_f}(t),\mathbf{q_i}(t_i)\right]\rho(0), \tag{41}$$

the equations of motion for the auxiliary density matrices can be calculated from (39) to give

$$\begin{aligned}\partial_t \rho_{\mathbf{n}}(t) = & -i\mathcal{L}\rho_{\mathbf{n}}(t) - \sum_{j,m} n_{j,m}\nu_{j,m}\rho_{\mathbf{n}}(t) \\ & -i\sum_{j,m} V_j^{\times}\left[\mathbf{q}(t)\right]\rho_{\mathbf{n}_{j,m}^{+}}(t)\end{aligned}$$

$$-i\sum_{j,m} n_{j,m}\left(c_{j,m}V_j\left[\mathbf{q}(t)\right]\right)^{\times}\rho_{\mathbf{n}^{-}_{j,m}}(t) \tag{42}$$

The Liouville space commutators defined at the fixed end point of the path $\mathbf{q}(t)$ can now be written at the operator level as $V^{\times}f = Vf - fV^{\dagger}$, for arbitrary operator f. This gives the final form of the hierarchy of equations of motion

$$\begin{aligned}\partial_t\rho_{\mathbf{n}}(t) \quad = \quad & -\left(i\mathcal{L}+\sum_{j,m} n_{j,m}\nu_{j,m}\right)\rho_{\mathbf{n}}(t) \\ & -i\sum_{j,m} V_j^{\times}\rho_{\mathbf{n}^{+}_{j,m}}(t) \\ & -i\sum_{j}\sum_{m} n_{j,m}\left(c_{j,m}V_a\right)^{\times}\rho_{\mathbf{n}^{-}_{j,m}}(t).\end{aligned} \tag{43}$$

The temperature correction terms in equation (18) arise by taking the Markov approximation $\nu_{j,m}\exp\left(-\nu_{j,m}\left(t-\tau\right)\right) \approx \delta\left(t-\tau\right)$ for the correlation function terms with $m > M$ and integrating equation

(27). With this approximation, $i\mathcal{L}$ is replaced by[36,42],

$$i\mathcal{L}' = i\mathcal{L} + \sum_j \sum_{m=M+1}^{\infty} \frac{c_{j,m}}{\nu_{j,m}} V_j^{\times} V_j^{\times}. \qquad (44)$$

References

[1] D. Xu and K. Schulten, in *The Photosynthetic Bacterial Reaction Center: II. Structure, Spectroscopy and Dynamics*, edited by J. Breton and A. Vermeglio (Plenum Press, New York, 1992), NATO Sci. Ser. A, pp. 301–312.

[2] Govindjee, in *Probing Photosynthesis: Mechanisms, Regulation, and Adaptation*, edited by M. Yunus, U. Pathre, and P. Mohanty (Taylor and Francis, New York, 2000), pp. 9–39.

[3] R. S. Knox, in *Primary Processes of Photosynthesis*, edited by J. Barber (Elsevier, Amsterdam, 1977), pp. 55–97.

[4] K. Sauer, in *Bioenergetics of Photosynthesis*, edited by Govindjee (Academic Press, 1975), pp. 115–181.

[5] M. K. Sener, J. D. Olsen, C. N. Hunter, and K. Schulten, Proc. Natl. Acad. Sci. USA **104**, 15723 (2007).

[6] R. Cogdell, N. Isaacs, A. Freer, J. Arrelano, T. Howard, M. Papiz, A. Hawthornthwaite-Lawless, and S. Prince, Progr. Biophys. Molec. Biol. **68**, 1 (1997).

[7] T. Pullerits and V. Sundström, Acc. Chem. Res. **29**, 381 (1996).

[8] R. E. Blankenship, M. T. Madigan, and C. E. Bauer, eds., *Anoxygenic Photosynthetic Bacteria* (Kluwer Academic Publishers, 1995).

[9] G. R. Fleming and R. van Grondelle, Curr. Opin. Struct. Biol. **7**, 738 (1997).

[10] M. K. Şener and K. Schulten, in *The Purple Phototrophic Bacteria*, edited by C. N. Hunter, F. Daldal, M. C. Thurnauer, and J. T. Beatty (Springer, 2008), vol. 28 of *Advances in Photosynthesis and Respiration*, pp. 275–294.

[11] X. Hu, T. Ritz, A. Damjanović, and K. Schulten, J. Phys. Chem. B **101**, 3854 (1997).

[12] J. Koepke, X. Hu, C. Muenke, K. Schulten, and H. Michel, Structure **4**, 581 (1996).

[13] O. Kühn, V. Chernyak, and S. Mukamel, J. Chem. Phys. **105**, 8586 (1996).

[14] X. Hu, T. Ritz, A. Damjanović, F. Autenrieth, and K. Schulten, Quart. Rev. Biophys. **35**, 1 (2002).

[15] V. Sundström, T. Pullerits, and R. van Grondelle, J. Phys. Chem. B **103**, 2327 (1999).

[16] V. I. Novoderezhkin and A. P. Razjivin, Chem. Phys. **211**, 203 (1996).

[17] V. I. Novoderezhkin and R. van Grondelle, J. Phys. Chem. B **106**, 6025 (2002).

[18] V. I. Novoderezhkin, D. Rutkauskas, and R. van Grondelle, Biophys. J. **90**, 2890 (2006).

[19] L. Valkunas, J. Janusonis, D. Rutkauskas, and R. van Grondelle, J. Luminesc. **127**, 269 (2007).

[20] M. Yang and G. R. Fleming, Chem. Phys. **282**, 163 (2002).

[21] V. May, Int. J. Quantum Chem. **106** (2006).

[22] O. Kühn and V. Sundström, J. Chem. Phys. **107**, 4154 (1997).

[23] T. Renger, V. May, and O. Kühn, Phys. Rep. **343**, 137 (2001).

[24] W. M. Zhang, T. Meier, V. Chernyak, and S. Mukamel, J. Chem. Phys. **108**, 7763 (1998).

[25] A. Ishizaki and G. R. Fleming, J. Chem. Phys. **130**, 234110 (2009).

[26] A. Damjanović, T. Ritz, and K. Schulten, Int. J. Quantum Chem. **77**, 139 (2000).

[27] Y. Tanimura and R. Kubo, J. Phys. Soc. Jpn. **58**, 1199 (1989).

[28] A. Ishizaki and G. R. Fleming, J. Chem. Phys. **130**, 234111 (2009).

[29] A. Ishizaki and G. R. Fleming, Proc. Natl. Acad. Sci. USA **106**, 17255 (2009).

[30] A. M. van Oijen, M. Katelaars, J. Köhler, T. J. Aartsma, and J. Schmidt, Science **285**, 400 (1999).

[31] S. Tretiak, C. Middleton, V. Chernyak, and S. Mukamel, J. Phys. Chem. B **104**, 9540 (2000).

[32] V. May and O. Kühn, *Charge and Energy Transfer Dynamics in Molecular Systems* (WILEY-VCH, Berlin, 2000).

[33] Y. C. Cheng and R. J. Silbey, J. Phys. Chem. B **109**, 21399 (2005).

[34] Y. Tanimura, J. Phys. Soc. Jpn. **75**, 082001 (2006).

[35] U. Weiss, *Quantum dissipative systems* (World Scientific Publishing Company, 2008).

[36] A. Ishizaki and Y. Tanimura, J. Phys. Soc. Jpn. **74**, 3131 (2005).

[37] R. X. Xu, P. Cui, X. Q. Li, Y. Mo, and Y. J. Yan, J. Phys. Chem. **122**, 041103 (2005).

[38] Y. J. Yan and R. X. Xu, Annu. Rev. Phys. Chem. **56**, 187 (2005).

[39] Y. Yan, F. Yang, Y. Liu, and J. Shao, Chem. Phys. Lett. **395**, 216 (2004).

[40] Y. Tanimura, Phys. Rev. A **41**, 6676 (1990).

[41] R. X. Xu and Y. J. Yan, Phys. Rev. E **75**, 031107 (2007).

[42] Q. Shi, L. Chen, G. Nan, R. Xu, and Y. Yan, J. Chem. Phys. **130**, 084105 (2009).

[43] M. Schröder, M. Schreiber, and U. Kleinekathöfer, J. Chem. Phys. **126**, 114102 (2007).

[44] I. Kosztin and K. Schulten, in *Biophysical Techniques in Photosynthesis II*, edited by T. Aartsma and J. Matysik (Springer, Dordrecht, 2008), vol. 26 of *Advances in Photosynthesis and Respiration*, pp. 445–464.

[45] A. Damjanović, I. Kosztin, U. Kleinekathoefer, and K. Schulten, Phys. Rev. E **65**, 031919 (2002), (24 pages).

[46] L. Janosi, I. Kosztin, and A. Damjanovic, J. Chem. Phys. **125**, 014903 (2006).

[47] U. Kleinekathöfer, J. Chem. Phys. **121**, 2505 (2004).

[48] O. Zerlauskiene, G. Trinkunas, A. Gall, B. Robert, V. Urboniene, and L. Valkunas, J. Phys. Chem. B **112**, 15883 (2008).

[49] A. Freiberg, M. Ratsep, K. Timpmann, and G. Trinkunas, Chem. Phys. **357**, 102 (2009).

[50] W. Liu, Y. Yan, K. Liu, C. Xu, and S. Qian, Front. Phys. China **1**, 283 (2006).

[51] S. Vulto, J. Kennis, A. Streltsov, J. Amesz, and T. Aartsma, J. Phys. Chem. B **103**, 878 (1999).

[52] H. M. Visser, O. J. G. Somsen, F. van Mourik, and R. van Grondelle, J. Phys. Chem. **100**, 18859 (1996).

[53] S. E. Bradforth, R. Jimenez, F. van Mourik, R. van Grondelle, and G. R. Fleming, J. Phys. Chem. **99**, 16179 (1995).

[54] A. Freiberg, V. I. Godik, T. Pullerits, and K. Timpmann, Biochim. Biophys. Acta **973**, 93 (1989).

[55] P. Herman, U. Kleinekathöfer, I. Barvík, and M. Schreiber, J. Luminesc. **94-95**, 447 (2001).

[56] G. Trinkunas and A. Freiberg, J. Luminesc. **119-120**, 105 (2006).

[57] J. Linnanto and J. Korppi-Tommola, Chem. Phys. **357**, 171 (2009).

[58] T. Ritz, S. Park, and K. Schulten, J. Phys. Chem. B **105**, 8259 (2001).

[59] M. Şener and K. Schulten, Phys. Rev. E **65**, 031916 (2002), (12 pages).

[60] S. Jang, M. D. Newton, and R. J. Silbey, Phys. Rev. Lett. **92**, 218301 (2004).

[61] G. D. Scholes, Annu. Rev. Phys. Chem. **54**, 57 (2003).

[62] R. van Grondelle and V. I. Novoderezhkin, Phys. Chem. Chem. Phys. **8**, 793 (2006).

[63] R. Monshouwer, M. Abrahamsson, F. van Mourik, and R. van Grondelle, J. Phys. Chem. B **101**, 7241 (1997).

[64] R. P. Feynman and F. L. Vernon, Jr., Ann. Phys. **24**, 118 (1963).